Preprints, 21st Conference on Severe Local Storms
12-16 August 2002, San Antonio, Texas

P10.1 TORNADOGENESIS IN A SIMULATED HP SUPERCELL

Catherine A. Finley*

Department of Earth Sciences - Meteorology
University of Northern Colorado, Greeley, Colorado

William R. Cotton and Roger A. Pielke Sr.

Department of Atmospheric Sciences
Colorado State University, Fort Collins, Colorado

1. INTRODUCTION

Much of our current understanding of the tornadogenesis process has come from visual storm observations (Lemon and Doswell, 1979), Doppler radar observations (Brandes, 1993) and field projects (Rasmussen et al., 1994). While field projects have provided valuable data in the near-tornado environment and portable Doppler radars are getting unprecedented wind observations in tornadoes (Wurman et al., 1996; Bluestein and Pazmany, 2000), it is still extremely difficult to get a three-dimensional observational data set capable of providing a complete picture of the tornadogenesis process.

Numerical models provide another tool for investigating the tornadogenesis process. Although there are some uncertainties in model results due to numerical issues and physical parameterizations, numerical models provide physically consistent three-dimensional data sets to study tornadogenesis. Previous modeling studies of tornadogenesis in supercell storms have focused on classic supercells in idealized horizontally homogeneous environments (Wicker and Wilhelmson, 1993, 1995). In this study, we extend previous work by investigating the tornadogenesis process in a simulated HP supercell which develops in an inhomogeneous environment.

2. EXPERIMENT DESIGN

A nested grid primitive equation model, RAMS v3b, (Pielke et al., 1992) was used to simulate an HP supercell and tornadic vortices. To better understand storm development and evolution in more realistic environments, the model was initialized with synoptic data from a case in which an HP supercell produced several weak (F0-F1) tornadoes over northeast Kansas (30 June, 1993). Six telescoping nested grids were used in the simulation, allowing for atmospheric flows ranging from synoptic-scale motions down to tornadic vortices to be represented. All convection in the simulation was initiated with resolved vertical motion and subsequent condensation/latent heating from the model microphysics; no warm bubbles or cumulus parameterizations were used. A summary of the horizontal grid configuration used in the simulation is shown below. All grids had 32 points in the vertical, with stretched vertical grid spacing starting at 80 m near the surface. The top of the model domain extended upward to 20 km. A more detailed description of the synoptic situation and the model configuration used in the simulation can be found in Finley et al., 2001.

TABLE 1: Horizontal grid configuration used in the simulation.

GRID 1	44 x 34 points	Δx = 120 km
GRID 2	44 x 50 points	Δx = 40 km
GRID 3	42 x 42 points	Δx = 8 km
GRID 4	57 x 57 points	Δx = 1.6 km
GRID 5	90 x 90 points	Δx = 400 m
GRID 6	202x202 points	Δx = 100 m

The model simulation was started at 12 UTC 30 June with Grids 1-3 to capture the early evolution of the synoptic features. Grid 4 was added at 20 UTC. During the next 4 hours, several supercells developed in Grid 4. Grids 5 and 6 were added at 00 UTC 1 July since it appeared that a smaller circulation started to develop on Grid 4 after this time.

This study focuses on the development and evolution of the tornadic vortices, and hence, all the results shown are from Grid 6. Since many vortices develop during the course of the simulation, we need to distinguish between tornadic and non-tornadic vortices. We will define a vortex as a 'tornado' when the following three conditions are simultaneously met on Grid 6:

1. A closed circulation (ground relative) exists at the lowest model level (z=38 m).
2. Winds $\geq$ 30 m s^{-1} exist somewhere within the closed circulation.
3. The maximum vertical vorticity at z=38 m exceeds 0.1 s^{-1} within the closed circulation.

3. RESULTS

The simulated HP supercell produced two separate tornadoes (as defined above – hereafter denoted as T1 and T2). A summary of some of the tornado characteristics is shown in Table 2. Horizontal cross sections of the wind field at different vertical levels and

* *Corresponding author address*: Dr. Cathy Finley, Dept. of Earth Sciences, Univ. of Northern Colorado, Greeley, CO 80639; email: cafinle@.unco.edu

times (not shown) indicated that both tornadoes

TABLE 2: Tornado characteristics.

	duration	max. wind speed	duration F1 winds
T1	0016–0022 UTC (44175 – 44520s)	34 m s^{-1} (0019 UTC)	3.75 min.
T2	0030–0031:30 UTC (45015 – 45060s)	34 m s^{-1} (0030:30UTC)	0.75 min.

developed first at the surface and then upward in time. T1 formed along the flanking line of the easternmost supercell (hereafter denoted as S1) to the southwest of the storm's mid-level mesocyclone. A well-defined weak mesoscale cyclonic circulation was present in the lower portion of the boundary layer prior to tornadogenesis, and tornadogenesis occurred near the center of this cyclonic circulation. Of special note is that the development of T1 coincided with a merger between the flanking line of S1 and another cell to the west (hereafter denoted as S2). During tornadogenesis, several separate downdrafts developed: an occlusion downdraft (round downdraft in the center of Fig. 1), a rear-flank downdraft (RFD - downdraft entering Fig. 1 from the left), and a third downdraft which appeared to be an intensification of the downdraft behind a solenoidal circulation. In time, the RFD merged with the downdraft to the southwest of the developing tornado forming one continuous downdraft which circled around the tornado. The occlusion downdraft remained separate throughout the development and lifetime of T1, and the vorticity maximum (and pressure minimum) was located along the vertical velocity gradient between strong updraft and occlusion downdraft (Fig. 1). However, surface winds did not reach tornadic strength (as defined above) until the RFD wrapped around the

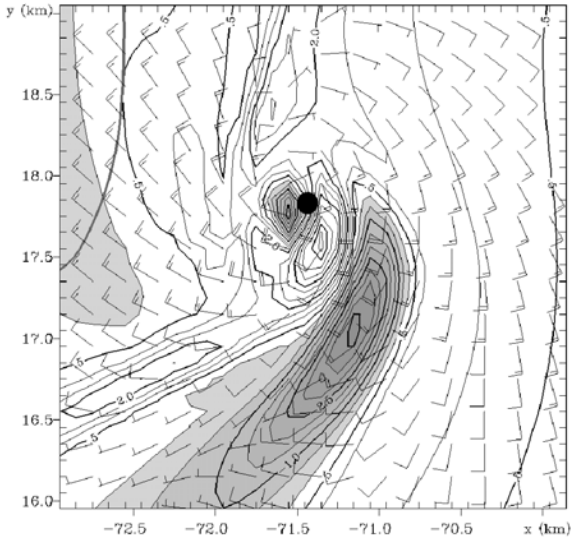

Fig. 1. Wind and vertical velocity (contour interval 0.5 ms^{-1}) at the lowest model level (z=38m) at 0013:30 UTC for a subset of Grid 6. Areas of downward motion are shaded. Wind barbs are plotted at every other grid point. The short (long) flag on the wind barb represents 5 ms^{-1} (10 ms^{-1}). The dot between the updraft and occlusion downdraft indicates the position of the maximum vorticity (and minimum pressure) in the developing tornado.

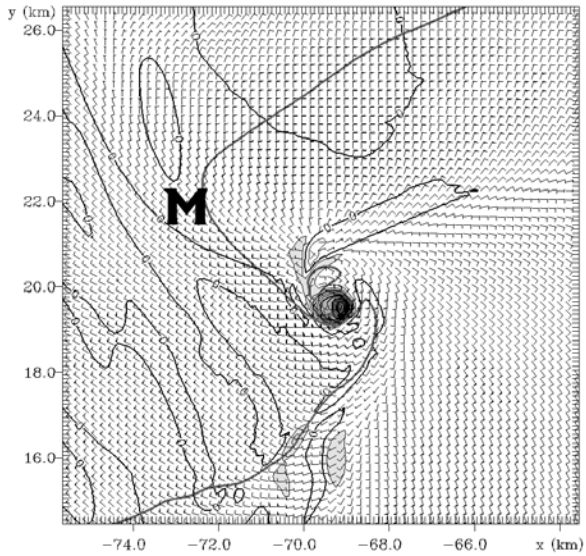

Fig. 2. Winds and vertical vorticity (contour interval 0.015 s^{-1}) for a subset of Grid 6 at the lowest model level at 0019:30 UTC. T1 is near its maximum intensity at this time. Areas of vertical vorticity exceeding 0.015 s^{-1} are shaded. Wind barbs are plotted at every other grid point. The short (long) flag on the wind barb represents 5 m s^{-1} (10 m s^{-1}). The position of the mid-level mesocyclone is indicated with an "M", and the 1 g(kg)$^{-1}$ condensate mixing ratio contour is denoted with a bold gray line.

developing vortex. Periodic RFD 'pulses' corresponded to periods of stronger wind speeds in the tornado. T1 lasted for almost 12 minutes, although the maximum winds dropped slightly below the tornadic threshold (down to a minimum of 28.4 m s^{-1}) in the middle of this time period. However, T1 was labeled as one tornadic event since a coherent vortex could be easily identified throughout the time period, and the minimum wind threshold for identifying tornadic vortices in the simulation is somewhat arbitrary.

To better understand the processes responsible for creating large vertical vorticity values near the surface during the development of T1, a vertical vorticity budget was calculated in the lowest model layer around the developing vortex. The vertical vorticity equation in flux form (neglecting terms involving planetary vorticity and diffusion) is given by:

$$\frac{\partial(\rho_o\zeta)}{\partial t} = -\frac{\partial(\rho_o u\zeta)}{\partial x} - \frac{\partial(\rho_o v\zeta)}{\partial y} - \frac{\partial(\rho_o w\zeta)}{\partial z} - \zeta\frac{\partial(\rho_o\zeta)}{\partial z} - \rho_o\left[\frac{\partial w}{\partial x}\frac{\partial v}{\partial z} - \frac{\partial w}{\partial y}\frac{\partial u}{\partial z}\right] \quad (1)$$

where ζ is the relative vertical vorticity and ρ_o is the base state density. To calculate the budget, each term in (1) was calculated in a volume 800 m x 800 m in the horizontal (corresponding to the distance between wind maxima on opposite sides of the vortex) x 80 m the vertical (the depth of the lowest model momentum

layer). The volume was centered on the maximum vertical vorticity value at the lowest model level, and the budget terms were calculated every 15 s.

Results from the budget calculation for T1 are shown in Fig. 3. The vertical black lines denote the genesis and dissipation times for T1. Stretching is the largest positive tendency during the genesis period, but tilting and horizontal advection also play a significant role in increasing the vertical vorticity in the box – particularly in the few minutes prior to tornadogenesis. Once T1 develops, horizontal vertical vorticity advection into the box appears significant in helping to maintain the tornado.

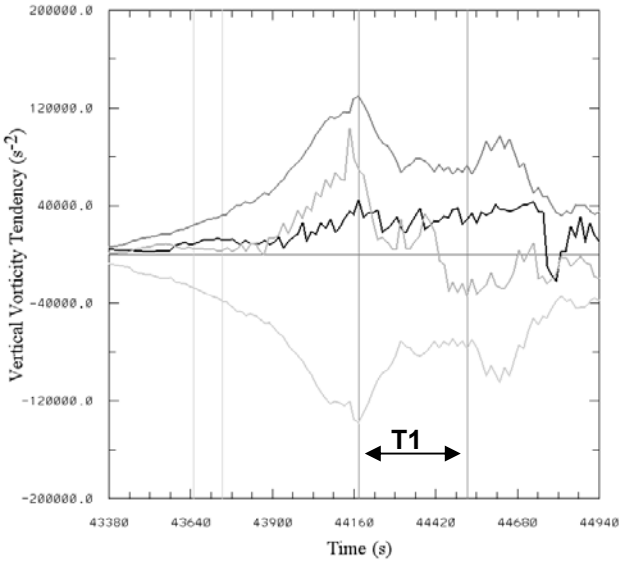

Fig. 3. Time evolution of the vertical vorticity tendencies integrated over an 800 m x 800 m x 80 m volume centered on the tornado at the lowest model level. The curves plotted are: total horizontal flux divergence (black), vertical flux divergence (light gray), tilting (medium gray), and convergence (dark gray). The black vertical lines indicate the times T1 developed and dissipated. The light gray vertical lines indicate the time period during which the occlusion downdraft developed at the lowest model level.

As mentioned above, the formation of T1 coincided with a merger between the flanking line of S1, and a storm to its west (S2). During the merger process, the updraft at midlevels intensified in the merger region, and tornadogenesis occurred on the north side of the enhanced updraft region. A time series of the maximum vertical vorticity at z=38 m and the average vertical velocity in a volume centered 4.3 km above the developing tornado is shown in Fig. 4. At approximately 0008 UTC (43680 s), the average vertical velocities above the tornadogenesis region increase rapidly and remain close to 15 ms^{-1} throughout the genesis period. Over the same time period, the vertical vorticity rapidly increases at the lowest model level, suggesting that enhanced low-level convergence may be responsible for this increase. The vorticity budget calculations indicate that the stretching tendency increases significantly throughout the time period. However, the occlusion downdraft also developed at the lowest model

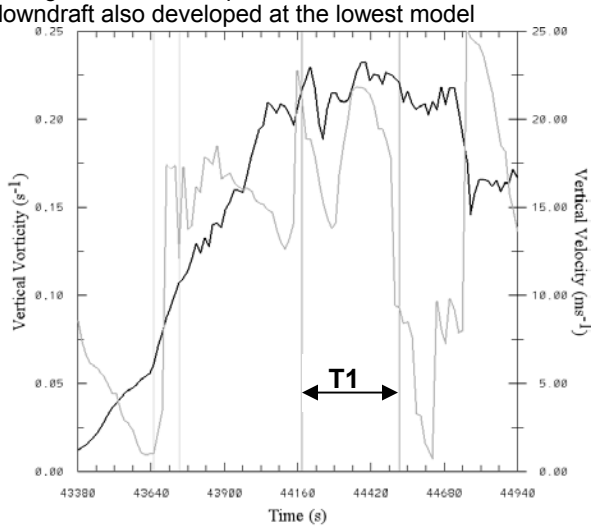

Fig. 4. Time series of the maximum vertical vorticity (black curve) at the lowest model level and the average vertical velocity in a 1 km x 1 km x 0.83 km volume 4.3 km above the surface centered over the developing tornado. The vertical lines are as in Fig. 3.

level at this time. Horizontal cross sections of the vorticity tendencies (not shown) revealed that low-level convergence is enhanced along the occlusion downdraft/updraft interface. Further analysis is needed to try to isolate the relative importance of the broader mesoscale convergence.

The second tornado (T2) developed in a region of strong cyclonic shear along the northern periphery of a strong westerly wind surge associated with the storm's transition into a bow echo (Figure 5). Although T2 developed beneath the 'rotating comma head' structure of the storm, T2 was not clearly connected with it. The fact that T2 only developed upward to a height of 2-3 km and developed very quickly suggests that a shearing instability mechanism may have played a role in its development.

A time series of the vertical vorticity at the lowest model level during the development of T2 is shown in Fig. 5. Several non-tornadic shearing instabilities formed along the leading edge of the outflow to the east of weakening T1. T2 developed west of T1 in a region of enhanced convergence and horizontal vertical vorticity advection. As the remnants of T1's vertical vorticity approached the broader shear zone, its vertical vorticity was extruded along the shear zone and advected toward T2 (see Fig. 5b). This evolution is similar to idealized modeling studies of shear instabilities and non-supercell tornadogenesis along outflow boundaries (Lee and Wilhelmson, 1997).

4. DISCUSSION

We have presented some preliminary analysis on the tornadogenesis process(es) in a simulated HP supercell. The first tornado (T1) developed along the

flanking line of the storm S1 and occurred shortly after the merger between the flanking line of S1 and another storm to the west. Tornadogenesis occurred along the northern edge of a strong mid-level updraft region that formed as the result of the merger, suggesting that enhanced surface convergence may have triggered tornadogenesis. Prior to tornadogenesis, a separate occlusion downdraft developed. T1 developed in the vertical velocity gradient between the occlusion downdraft and a strong updraft. The second tornado (T2) developed beneath the rotating-comma head portion of the storm as the storm transitioned into a bow echo, and appeared to develop as a result of a shearing instability.

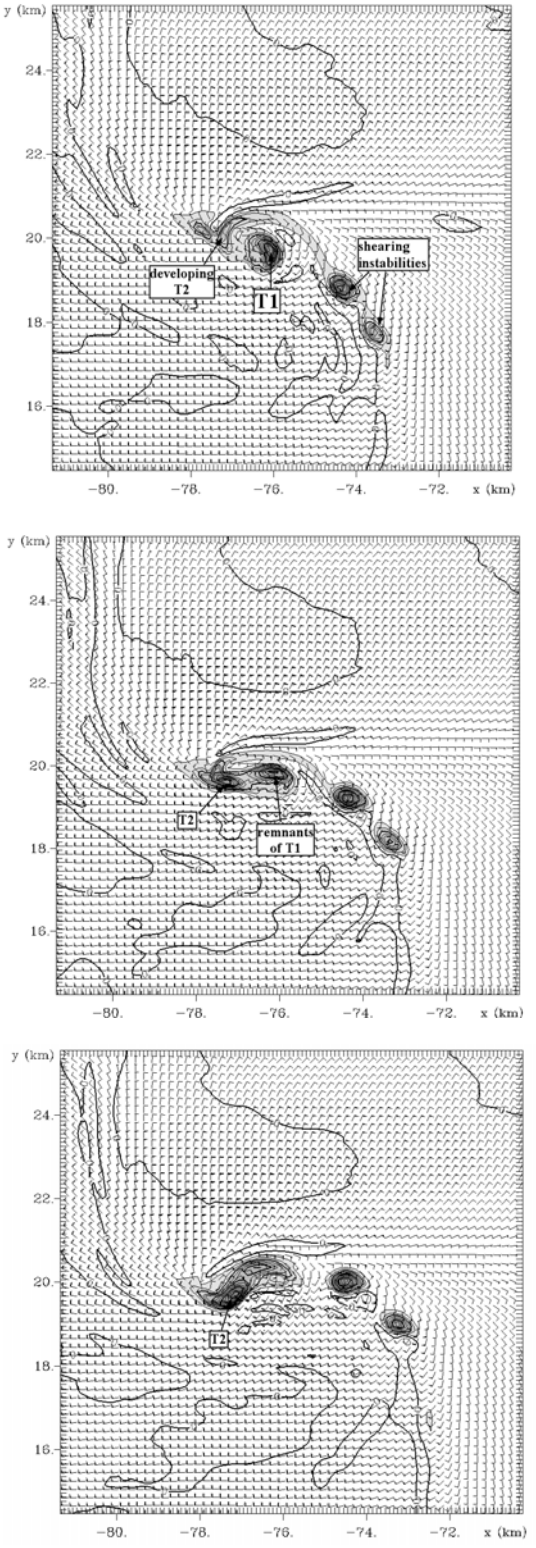

Fig. 5. Winds and vertical vorticity (contour interval 0.015 s^{-1}) at the lowest model level during the development of T2 at (a) 0028:30 UTC, (b) 0029:30 UTC and (c) 0030:30 UTC. Vertical vorticity exceeding 0.015 s^{-1} is shaded. Wind barbs are plotted at every other grid point. The short (long) flag on the wind barb represents 5 ms^{-1} (10 ms^{-1}).

The model results raise some interesting questions. Does the occlusion downdraft cause tornadogenesis, or is it an artifact of the tornadogenesis process? Is there a dynamical connection between the occlusion downdraft and the RFD? These questions are currently under investigation.

5. ACKNOWLEDGEMENTS

This research was supported by the National Science Foundation under grants ATM-0105279, ATM-9910857 and ATM-9900929.

6. REFERENCES

Bluestein, H.B. and A.L. Pazmany, 2000: Observations of tornadoes and other convective phenomena with a mobile, 3-mm wavelength doppler radar: the spring 1999 field experiment. *Bull. Amer. Meteor. Soc.,* **81**, 2939-2950.

Brandes, E.A., 1993: Torandic thunderstorm characteristics determined with doppler radar. *The Tornado: Its structure, dynamics, prediction, and hazards. Geophys. Monogr.*, No. 79, Amer. Geophys. Union, 143-159.

Finley, C.A., W.R. Cotton, and R.A. Pielke Sr., 2001: Numerical simulation of tornadogenesis in a high-precipitation supercell. Part I: Storm evolution and transition into a bow echo. *J. Atmos. Sci.*, **58**, 1597-1629.

Lee, B. D., and R. B. Wilhelmson, 1997: The numerical simulation of non-supercell tornadogenesis. Part II: Evolution of a family of tornadoes along a weak outflow boundary. *J. Atmos. Sci.*, **54**, 2387-2415.

Lemon, L.R., and C.A. Doswell III, 1979: Severe thunderstorm evolution and mesocyclone structure as related to tornadogenesis. *Mon. Wea. Rev.,* **107**, 1184-1197.

Pielke, R.A., W.R. Cotton, R.L. Walko, C.F. Tremback, W.A. Lyons, L.D. Grasso, M.E. Nicholls, M.D. Moran, T.J. Lee, and J.H. Copeland, 1992: A comprehensive meteorological modeling system-RAMS. *Metero. And Atmos. Phys.,* **49**, 69-91.

Rasmussen, E.N., J.M. Straka, R. Davies-Jones, C.A. Doswell, F.H. Carr, M.D. Eilts, and D.R. MacGorman, 1994: Verification of the origins of rotation in tornadoes experiment: VORTEX. *Bull. Amer. Meteor. Soc.,* **75,** 995-1006.

Wicker, L.J., and R. B. Wilhelmson, 1993: Numerical simulation of tornadogenesis within a supercell thunderstorm. *The Tornado: Its structure, dynamics, prediction, and hazards. Geophys. Monogr.*, No. 79, Amer. Geophys. Union, 75-88.

Wicker, L.J., and R. B. Wilhelmson, 1995: Simulation and analysis of tornado development and decay within a three-dimensional supercell thunderstorm. *J. Atmos. Sci.,* **52**, 2675-2703.

Wurman, J., J.M. Straka, and E.N. Rassmussen, 1996: Fine-scale

Doppler radar observations of tornadoes. *Science*, **222**, 1774-1777.